

# The robust assembly of small symmetric nano-shells

Jef Wagner\*, Roya Zandi\*

\*Department of Physics and Astronomy, University of California, Riverside, 900 University Ave,  
Riverside, California 92521, USA

## Abstract

Highly symmetric nano-shells are found in many biological systems, such as clathrin cages and viral shells. Several studies have shown that symmetric shells appear in nature as a result of the free energy minimization of a generic interaction between their constituent subunits. We examine the physical basis for the formation of symmetric shells, and using a minimal model we demonstrate that these structures can readily grow from identical subunits under non equilibrium conditions. Our model of nano-shell assembly shows that the spontaneous curvature regulates the size of the shell while the mechanical properties of the subunit determines the symmetry of the assembled structure. Understanding the minimum requirements for the formation of closed nano-shells is a necessary step towards engineering of nano-containers, which will have far reaching impact in both material science and medicine.

Submitted July 16th, 2014.

\*Correspondence:

## 1 INTRODUCTION

The spontaneous assembly of building blocks into complex ordered structures is ubiquitous in nature. Examples include the formation of symmetric shells with extraordinary accuracy such as clathrin vesicles for membrane trafficking in cells and viral shells for the protection and transportation of viral genome. Based on very basic physical principles, it has been argued that small spherical viruses display structures with icosahedral symmetry(1), and while some larger clathrin vesicles are irregular in shape, the smallest clathrin shells observed *in vitro* tend to take on a discrete set of symmetric structures(2). Figure 1 shows the 3D image reconstructions of enterovirus 71, an icosahedral virus(3) and a  $D_6$  symmetric clathrin coat(4) obtained through the use of spatial averaging over the set of associated symmetries.

The simplicity and highly symmetric shape of viral shells with diameters ranging from 20 to 120 *nm* have in particular attracted the attention of scientists for many decades(5–11). The simplest viruses are made of a genome encapsulated in a protein shell called the capsid. Quite remarkably, under many circumstances, the viral coat proteins assemble spontaneously around its genome or other negatively charged cargoes to form capsids identical to those observed *in vivo*(12–16). Despite the importance of engineered biological nano-shells in gene and drug delivery and other biomedical technologies, the mechanisms and factors that control the structure and stability of shells made of identical building blocks are just beginning to be understood. Constructing the building blocks with interactions similar to those in the natural nano-containers may lead to the fabrication and design of precise synthetic nano-structures (11, 17, 18).

There have been many studies investigating the equilibrium shapes of shells formed from one or two identical subunits under external constraints(7–9, 11, 16, 19–22). The simple case of spherical colloids or circular disks constrained to reside on the surface of a sphere shows that the stability of formed shells depends strongly on the number of assembly subunits and interactions between them. For example, the solutions of the optimal packing problem of  $N$  identical hard disks on the surface of a sphere, known as the Tammes problem, reveal the presence of a number of local maxima in the plot of the sphere coverage vs. number of disks,  $N$ . The structures characterized by “Magic Numbers”,  $N = 12, 24, 32, 44, \dots$  corresponding to the local maximum coverage often have higher symmetry than their neighboring structures(8). A different set of magic numbers appear when minimizing the free energy of the  $N$  identical disks interacting through Lennard Jones potential. Some of these magic numbers and their associated shells coincide with the number of capsomers (protein multimers) in structures

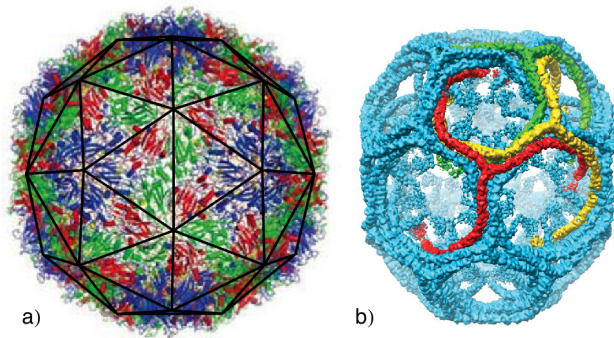


Figure 1: (color online) Images of (a) a viral shell (enterovirus 71) and (b) a small clathrin coat. The viral shell is a T=3 icosahedral virus, constructed of 180 identical protein subunits. The proteins sit in three color coded quasi-equivalent positions, grouped into triangles as seen with the dark outline in subfigure (a). The clathrin coat (b) has a  $D_6$  dihedral symmetry and is often referred to as a  $D_6$  barrel. The clathrin molecules have a triskelion (three legged) shape, that bind anti-parallel leg-to-leg. The symmetries displayed by these shells allow for very detailed imaging through the technique of spatial averaging.

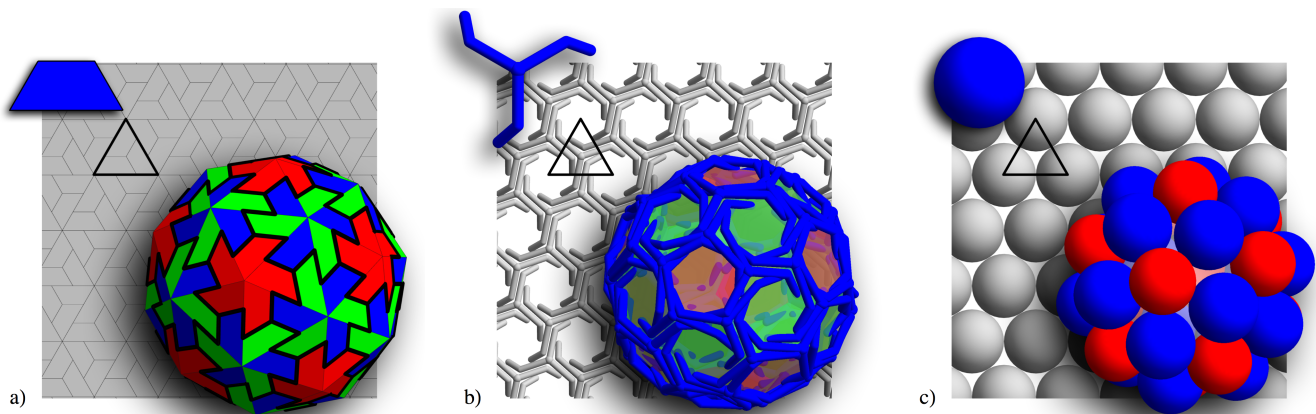


Figure 2: (color online) Three different systems that display a shell with the exact same symmetry. The black triangle in the background of each subfigure highlights the triangular subunits. Shell (a) is constructed of trimers similar to the viral shells, shell (b) is a soccer ball clathrin coat constructed from triskelion molecules, and shell (c) is built of small spheres connected through Lennard Jones potential with a convexity constraint. As seen in the background, all the subunits display a local hexagonal symmetry if packed onto a flat surface.

displaying icosahedral symmetry. Magic numbers corresponding to non-icosahedral shells with octahedral and cubic symmetries also appear in Monte Carlo simulations of disks sitting on the surface of a sphere(7, 8), consistent with the structures observed in virus assembly experiments performed *in vitro*.

The same magic numbers and structures were observed in the Monte Carlo simulations of the self-assembly of cone-shaped particles with attractive interactions(11). The authors in Ref. (11) showed that over a range of cone angles, a unique precise sequence of robust clusters form under equilibrium conditions. Note that the self-assembly of attractive spheres under a spherical convexity constraint reproduces exactly the same sequence of shells(23). The structure and symmetry of the small cluster sizes in these simulations(11, 23) were identical to those observed in the experimental studies of evaporation-driven assembly of colloidal spheres(17).

Quite interestingly, some of these magic numbers also appeared in completely different experiments, which showed that under appropriate conditions clathrin molecules spontaneously assemble *in vitro* to form highly symmetric vesicles whose radii depend on the size of cargoes(2). The fact that in distinct systems we observe shells with identical symmetry reveals the existence of a common underlying design principle governing the assembly of these structures.

One can readily observe that the building blocks of all the aforementioned systems can be packed with hexagonal symmetry in a flat space. This is clearly illustrated in Fig. 2, which shows a viral capsid, a clathrin vesicle, and a shell constructed of spheres, all with their associated building blocks. All shells in Fig. 2 have icosahedral symmetry. While defect free stacks of hexagonal layers in the 3 dimensional space can easily grow from interacting Lennard Jones particles under non-equilibrium conditions, a closed shell requires the formation of 12 defects with local fivefold rotational symmetry (pentamers). In symmetric shells the position of pentamers with respect to each other is precise, *i.e.*, the symmetry can be readily broken if one pentamer is slightly misplaced. One would then expect that the assembly of highly symmetric shells proceeds reversibly. In fact, most previous studies and simulations were done assuming the process of assembly is completely reversible, the switching between pentamers and hexamers can easily take place when necessary(10, 15, 24–27).

In this paper, we investigate the growth of a shell by subunits that can connect together with a local hexagonal symmetry. Despite the sensitivity of the symmetry of shells to the exact location of pentamers, under many experimental conditions the self-assembly of perfect icosahedral virus capsids is robust and efficient. The robustness of the process raises the question of whether a fully reversible assembly pathway is necessary for the formation of symmetric nano-containers. To this end, we develop a simple model to investigate the assembly of shells constructed from identical subunits with the minimum set of designing principles for irreversible growth. Unexpectedly, we find that the shells under non-equilibrium conditions grow to form the highly symmetric structures (see Figs. 5, 6, and 7 below) observed in biological systems and in equilibrium studies(7, 11, 23).

It is important to note that while there is a striking similarity between the aforementioned disparate systems, there are also significant differences. Viral capsids *in vivo* tend to only form structures with icosahedral symmetry, while the clathrin molecules as well as conical particles form shells with additional symmetries. The goal of the paper is to explain the basis of the similarities and differences displayed in nature’s nano-containers. According to our studies, the differences in these systems are the result of the distinct mechanical properties of their constituent building blocks. Our findings elucidate the kinetic pathways of assembly and fundamental packing principles in curved space observed in the distinct biological structures.

## MODELS AND METHODS

To study the kinetic pathways of the shell growth, we employed triangular subunits, which can represent either a trimer of viral capsid proteins, a triskelion molecule, or locus of three disks, see the highlighted triangles in Fig. 2. In the model, the growth proceeds through the irreversible addition of the triangular subunits to the exterior edges of the incomplete shell. After the addition of each subunit, the elastic sheet is allowed to relax and to find its minimum energy configuration. The minimization of the elastic energy of the growing shell is done numerically using a non-linear conjugate gradient method(28).

The 2-dimensional growing shell is a bond network built from triangles representing the smallest subunit of the shell, see Fig. 3a. While the subunit in Fig. 3a corresponds to the locus of three disks, any other trimers illustrated in Fig. 2 could be used. The energy of the triangular shell can then be separated into the bond stretching and bending energies(6, 9). The stretching energy comes from deforming the subunits from the preferred shape of an equilateral triangle, and is modeled by considering each bond as a linear spring with spring constant  $k_s$ . The stretching energy is then simply a sum of the deformation energy

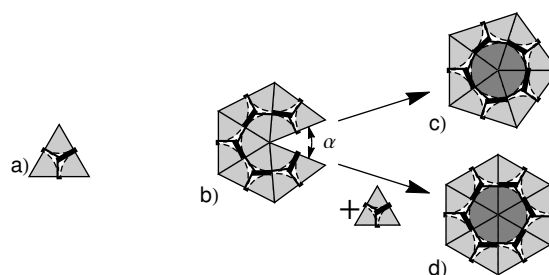


Figure 3: A subunit illustrated as an equilateral triangle (a). The subunits bond together edge to edge, and the growth of the shell proceeds by adding the subunit to the location with the smallest opening angle,  $\alpha$  (b). As the shell grows, the two unbound edges can either bind together to form a pentamer (c), or a new subunit can be added and bound along both edges to form a hexamer (d). The choice between forming a pentamer and a hexamer is based on which leads to a lower energy per subunit in the growing shell.

over all triangles

$$E_s = \sum_i \sum_{a=1}^3 \frac{k_s}{2} (b_i^a - b_0)^2. \quad (1)$$

where  $i$  indexes the triangular subunits,  $b_0$  is the equilibrium length of the bonds, and  $b_i^a$  is the length of the  $a^{\text{th}}$  bond in the  $i^{\text{th}}$  subunit. The bending energy results from the deviation of local radius of curvature from the preferred one and is calculated by summing over all neighboring pairs of triangular subunits

$$E_b = \sum_{\langle ij \rangle} k_b (1 - \cos(\theta_{ij} - \theta_0)), \quad (2)$$

where  $\langle ij \rangle$  indexes pairs of joined subunits,  $k_b$  is the torsional spring constant, and  $\theta_0$  is the preferred angle between two subunits determined by the spontaneous radius of curvature  $R_0$ . The angle between neighboring subunits,  $\theta_{ij}$ , is defined by the relation  $\cos \theta_{ij} = \hat{n}_i \cdot \hat{n}_j$ , where  $\hat{n}_i$  is the normal vector for the  $i^{\text{th}}$  subunit. The preferred angle  $\theta_0$  is defined as the angle between the normal vectors of two equilateral triangles sharing a side of length  $b_0$  and whose vertices sit on a sphere of radius  $R_0$ . The explicit relation between the preferred angle and radius of curvature is  $\sin \theta_0/2 = (12R_0^2/b_0^2 - 3)^{-1/2}$ .

The total energy of the two dimensional bond network depends upon two dimensionless parameters,  $\bar{\gamma} = k_s b_0^2/k_b$  and  $R_0/b_0$ . The parameter  $\bar{\gamma}$ , the Foppl von Karman (FvK) number, presents the relative difficulty of deforming a subunit from its equilateral triangular shape vs. the difficulty of bending away from the preferred radius of curvature. The second dimensionless parameter  $R_0/b_0$  is simply the spontaneous radius of curvature. Note that the FvK number in this work is normalized with respect to size of the subunits  $b_0$ .

The shell is assumed to grow along the minimum free energy path, so at each growth step a new subunit is added to the growing edge such that it maximizes the number of neighbors at the vertices of the newly accreted subunit. This is accomplished in practice by adding the new subunit to the location with the smallest opening angle  $\alpha$ , see Fig. 3b. If a vertex on the edge of a growing shell has already 5 triangles attached then the assembly could proceed in two different ways: (i) joining the two neighboring edges without adding a new subunit and thus forming a pentamer as in Fig. 3c, or (ii) inserting a new subunit and constructing a hexamer as in Fig. 3d. The choice between forming a pentamer or a hexamer is made based on which configuration induces a lower energy per subunit in the elastic sheet.

In addition to the deterministic simulations described above, we introduced stochasticity into the simulated growth. For the deterministic growth each subunit is added to the location with the smallest opening angle,  $\alpha$ . However, for the stochastic model, each position for addition of next protein is weighted based on the following criteria: (i) the smallest opening angle is considered the most probable one, (ii) opening angles within some range ( $\alpha + \sigma$ ) of the minimum are assumed to be about equally probable, and (iii) the opening angles much larger than the minimum should be very unlikely. A Gaussian weighting function  $w_i$  centered on the minimum angle,  $\alpha$  with width  $\sigma$  has all these properties

$$w_i = e^{-\frac{1}{2} \frac{(\alpha_i - \alpha)^2}{\sigma^2}}, \quad (3)$$

with  $\alpha_i$  the opening angle at the  $i^{\text{th}}$  vertex along the exterior edge. The location of the new subunit is then randomly chosen from the weighted list of possible locations. In the stochastic model we still let the shell relax and reach its minimum elastic energy configuration after the addition of each subunit, and choose between pentamers and hexamers in the same manner as in the deterministic model. It can be noted at this point that the deterministic model is simply the stochastic model in the limit as  $\sigma$  approaches zero. For nonzero  $\sigma$  the stochastic nature of this second model allows for the possibility of multiple different shells to be grown from the same set of parameters.

## RESULTS AND DISCUSSION

We investigated the growth of shells as described in the previous section for several values of dimensionless parameters  $0.1 < \bar{\gamma} < 10$  and  $1.1 < R_0/b_0 < 1.8$ . As illustrated in Fig. 4, we found that over a large range of parameter space, only a few different structures formed. Most of these structures had high symmetry and were robust, insensitive to small changes in the subunit's spontaneous radius of curvature or mechanical properties. The shaded regions labeled (A) through (H) in Fig. 4 correspond to the symmetric shells presented in Figs. 5, 6 and 7, plotted with the subunits shown in Figs. 2b, 2a, and 2c, respectively. The reason we plotted the shells with different types of subunits will become clear below. All symmetric shells are shown together with the same type of subunit in Fig. A.1 in the appendix. The number of subunits  $n_s$  and vertices  $N$  for each structure are given in the caption of Fig. A.1.

To investigate the effect on the shell size of FvK number and the spontaneous radius of curvature we first studied in detail the growth of small shells for a fixed value of the FvK number and a range of spontaneous radius of curvatures. Note that the

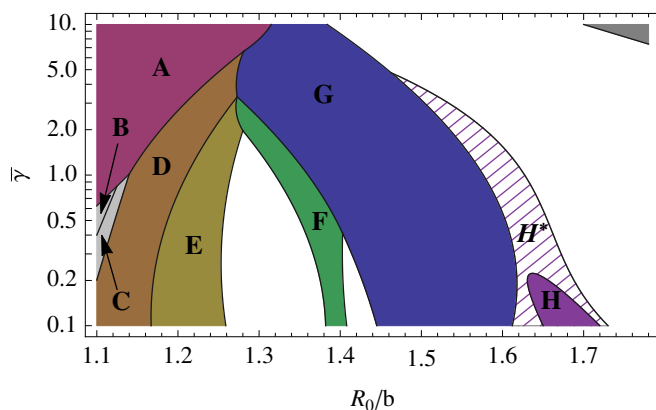


Figure 4: (color online) A parameter space plot for the deterministic model showing the different kind of shells grown for values of the dimensionless parameters  $\bar{\gamma}$  and  $R_0/b_0$ . The dark shaded contiguous regions labeled by letters (A) through (H) correspond to regions where only a single type of symmetric shell is grown. These structures are shown in Figs. 5, 6, and 7. In region labeled (H\*), in addition to a symmetric shell, several similarly sized non-symmetric shells assembled. The white areas correspond to regions in which different types of shells without any specific symmetry are grown. The unlabeled dark shaded region in the upper left corner of the plot with large FvK number and large spontaneous radius of curvature corresponds to a region in which no pentamers can be formed and the elastic sheet curves around to form a cylinder.

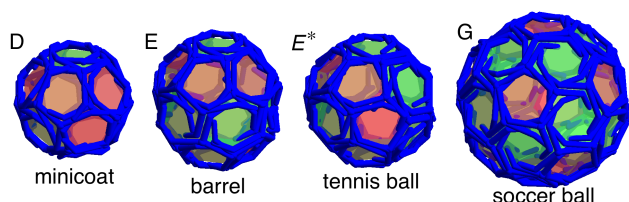


Figure 5: (color online) Structures presented with the three legged triskelion subunits. These shells are very similar to clathrin coats. Of particular interest are the symmetric shells seen in *in vitro* studies of empty clathrin coats, such as the minicoat with 28 subunits and tetrahedral symmetry (D), the hexagonal barrel with 36 subunits and  $D_6$  dihedral symmetry (E), the a tennis ball with 36 subunits and  $D_2$  symmetry ( $E^*$ ), and a soccer ball with 60 subunits and icosahedral symmetry (G). The (D), (E), ( $E^*$ ), and (G) structures correspond to the labeled regions in Figs. 4 and 11. The open faces are shaded red if they have five sides or green in case of six sides. Note that ( $E^*$ ) only appears in stochastic simulations (see the text).

FvK number is the ratio of the stretching to bending modulus, and as such a large FvK number corresponds to a system in which the subunits significantly resist deformation from the shape of an equilateral triangle, while a small one corresponds to a system in which the subunits can be easily deformed.

The results of our simulations for an intermediate value of FvK number  $\gamma = 2$  are plotted in Fig. 8, which shows the average radius of completed shells vs. the spontaneous radius of curvature. The stair-step like feature in Fig. 8 shows that we found a discrete set of shells, formed according to the spontaneous radius of curvature. In general for FvK numbers  $\gamma > 1.5$ , as the spontaneous radius of curvature increased, we observed discrete jumps from one symmetric shell type to another.

Figure 5 illustrates some of the structures associated with the labelled flat steps in Fig. 8 for  $\gamma = 2$ . These shells are similar to those observed in clathrin vesicles: the minicoat, the hexagonal barrel, the tennis ball, and the soccer ball shells described in Fig. 5. The subunit of clathrin shells is a triskelion molecule, shown in the upper left corner of Fig. 2b, whose legs bond anti-parallel. While the molecules are relatively stiff, the long legs as well as the variability of the bond angle between the legs can lead to an intermediate FvK number  $\gamma = 2$ , and as a consequence a range of shells as seen in Fig. 5 are grown. It is believed that the radius of curvature of the clathrin shells is determined by the cargo(4) explaining further the variability of the bond angle and the small FvK number. For empty clathrin vesicles, it should be the preferred spontaneous curvature between clathrin subunits that defines the size of the smallest clathrin shells observed in the experiments, the so-called minicoat vesicle with 28 subunits, and not a dodecahedron with 20 subunits.

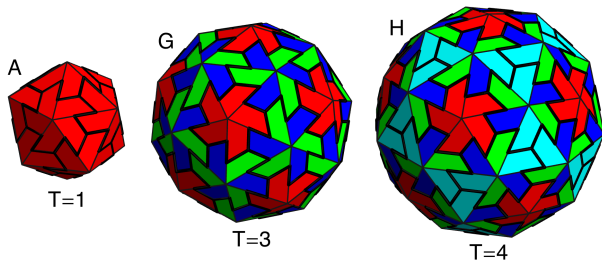


Figure 6: (color online) There are three shells that are grown with icosahedral symmetry, reminiscent of viral shells. These shells contain (A) 20, (G) 60, and (H) 80 subunits corresponding to  $T=1$ ,  $T=3$ , and  $T=4$  viral shells based on the Caspar-Klug classification of icosahedral shells. Larger icosahedral shells are not seen in simulated non-reversible growth model, perhaps explaining why scaffolding is needed for all larger icosahedral viruses.

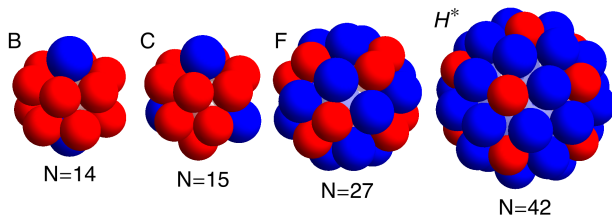


Figure 7: Additional shells that match the results of simulations presented in Chen *et al.* (11, 23). These include (b)  $N=14$  with  $D_{5h}$  symmetry, (c)  $N=15$  with  $D_{3h}$ , (g)  $N=27$  with  $S_6$  symmetry, and ( $h^*$ )  $N=42$  with  $D_{5h}$  symmetry.

Figure 8 also shows that for FvK number  $\gamma = 2$ , as the spontaneous radius of curvature increased beyond  $R_0/b_0 > 1.55$ , irregular shells without any underlying symmetry were assembled. An example of such an irregular shell is shown in the inset of Fig. 8. The irregular shells in this regime are more spherical in comparison to those with a larger FvK number as discussed below, and average radius of the completed shells closely matches the spontaneous radius of curvature of the subunits.

In contrast to clathrin vesicles and the shells obtained in theoretical simulations constructed from cones, spheres, or disk (7, 11, 23), which assemble into shells with different symmetries, viruses seem to only form structures with icosahedral symmetry *in vivo*. To explain this feature, we varied the FvK number and examined in detail its role on the shell symmetry. Our findings show that the FvK number can indeed explain the difference between shells appearing in viral capsids vs. clathrin coats.

For a fixed large FvK number  $\gamma = 10$ , the size of shells grown as a function of the spontaneous radius of curvature is illustrated in Fig. 9. We found two large flat regions, where rather considerable changes in spontaneous radius of curvature have no effect at all on the size of shell. These two flat steps correspond to the shells A and G with icosahedral symmetry shown in Fig. 6. If the subunits are considered as capsid protein trimers these correspond to  $T=1$  and  $T=3$  icosahedral shells based on the Caspar-Klug classification, see Fig. 6. As the spontaneous radius of curvature was increased  $R_0/b > 1.38$ , we found that large irregular oblong and ellipsoidal shells formed as illustrated in the inset to Fig. 9. As the spontaneous radius of curvature was increased even further the formation of pentamers (which are required in order to form closed shells) was suppressed completely, and only rolled flat sheets were grown.

Comparison of Figs. 8 and 9 shows that the more flexible subunits (lower FvK number) allowed for a larger variety of shells to grow. In fact, Fig. 4 shows that for  $\gamma = 0.5$  a few more structures in addition to those associated with clathrin vesicles ( $\gamma = 2$ ) or viral shells ( $\gamma = 10$ ) were grown. These additional structures are plotted in Fig. 7. Interestingly these shells were also observed in the molecular dynamic simulation of conical particles (11) or spherical particles with convexity constraints (23) as explained in the introduction. As the FvK number was decreased  $\gamma < 1.5$ , a new behavior emerged: The sharp transition between shell types (E) and (F) disappeared, and as the FvK number was further decreased below  $\gamma < 0.4$  the sharp transition between shell types (F) and (G) also disappeared, see Fig. 10. In between these regions small relatively spherical non-symmetric shells whose radii closely match the spontaneous radius of curvature were grown.

Our results illustrated in Figs. 4, 8, 9, and 10 clearly show that icosahedral structures are robust and appeared for all values of FvK numbers. The fact that most small spherical viruses only adopt  $T=1$  and  $T=3$  icosahedral structures and not



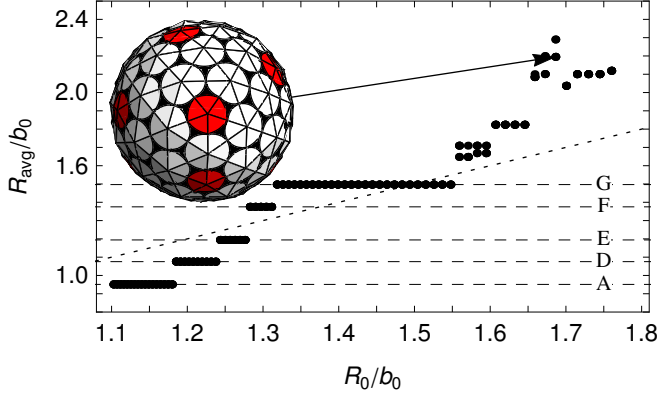


Figure 8: A plot of the average radius  $R_{avg}/b_0$ , defined as the radius of gyration of the vertices of the shell, versus the spontaneous radius of curvature  $R_0/b_0$ . The FvK number was fixed at a smaller value of  $\bar{\gamma} = 2$ , which corresponds to a mildly flexible subunit. The average radius of the symmetric shells (A), (D), (E) (F) and (G) are shown with the horizontal dashed lines. It is possible to see a stair step like feature with each flat step corresponding to a single type of symmetric shell. With the exception of the shells (A) and (F), the corresponding shell types are all seen in studies of empty clathrin coats performed *in vitro*. Representative shells are shown in Fig. 5. Note that the small radius of curvature of the shell (A) and the unreliable formation of shell (F) in the stochastic simulations could explain the absence of these shells in the experiments.

other symmetric shells illustrated in Figs. 5 and 7 indicate that viral coat proteins should take on a rigid tertiary structure and be difficult to deform as it is the case of  $\gamma = 10$  structures illustrated in Fig. 9.

It is interesting to note that only at the smaller FvK numbers,  $\bar{\gamma} < 0.25$ , we observed the  $n_s = 80$  icosahedral shell, corresponding to a T=4 capsid in the Caspar-Klug classification, see Fig. 6. We found two other structures with  $n_s = 80$  subunits at intermediate FvK numbers,  $0.25 < \bar{\gamma} < 2$ . However these shells either displayed a 5-fold  $D_5$  symmetry or no symmetry at all. The two non-icosahedral  $n_s = 80$  shells were not as spherical as the icosahedral one. The  $D_5$  structure (Fig. 7H\*), corresponding to the  $N = 42$  magic number shells also seen in Refs. (11, 23), was slightly prolate spheroidal, while the completely non-symmetric structure was ellipsoidal. It is worth mentioning that while icosahedral structures corresponding to  $n_s = 20$  and  $n_s = 60$  covered large areas of the parameter space in Fig. 4 and are still robust in the stochastic growth model (see below), the  $n_s = 80$  icosahedral shell only appeared in a small region of the phase space and was not as robust. This might indicate that forming a T=4 capsid with triangular subunits similar to those employed in the simulations done in this paper is difficult. Also this could explain the relevant abundance of T=1 and T=3 icosahedral virus capsids compared to the T=4 ones observed in nature. Note that  $N=42$  icosahedral structures did not appear in the simulations of Refs. (11, 23) (instead they found the  $D_5$  shell mentioned above) and appeared in Ref. (7) only if the overall system was under pressure.

In addition to the deterministic simulations, we studied the growth of shells for the stochastic model with the width of the distribution  $\sigma = 20^\circ$  (see Eq. 3), which was the smallest value of  $\sigma$  for which there was an appreciable difference between the stochastic and deterministic models. We found that the symmetric shells still reliably grew in the stochastic model exactly in the same regions as they appeared in the deterministic one, as shown in Fig. 11. This indicates that the stochastic choice of where to add the next subunit did not have a strong effect on the final structure of the symmetric shells. This was not, however, the case for the irregular shells that correspond to the white areas of Fig. 4. In these regions of parameter space multiple and new irregular shells were formed compared to the structures assembled in the deterministic model.

There were a few exceptions to the robustness of the assembly of symmetric shells in the stochastic model. Both the  $N = 27$  (Fig. 7F) and T=4 (Fig. 6H) shells were not reliably formed in the stochastic growth model in that, in addition to the symmetric structures, similar sized non-symmetric shells were formed in the same region of parameter space. Further, one additional symmetric shell was observed in the stochastic model that did not appear in the deterministic one; the tennis ball shell (Fig. 5E\*). The barrel (Fig. 5E) and tennis ball both have the same number of clathrin subunits,  $n_s = 36$ , which consist of 12 pentagonal and 8 hexagonal faces. Shell (E), which was the only shell seen with  $n_s = 36$  in the deterministic simulation, contains two rings of six pentagons separated by a ring of 6 hexagons. Shell (E\*) has the 12 pentagons all connected in a line that winds around the shell in the same manner as the seam on a tennis ball, and the 8 hexagons lay in two patches of 4. Note that both structures were observed in the experimental studies of assembly of clathrin coats(2).

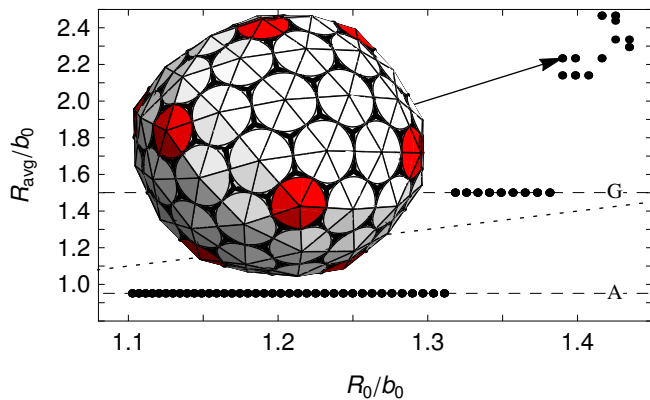


Figure 9: A plot of the average radius  $R_{\text{avg}}/b_0$  versus the spontaneous radius of curvature  $R_0/b_0$ . The FvK number is fixed at a large value of  $\bar{\gamma}=10$  corresponding to a very stiff subunit (difficult to deform). The two large flat regions seen in the plot correspond to small icosahedral structures shell types (A) (G) in Fig. 6. For spontaneous radius of curvatures larger than  $R_0/b_0 > 1.38$ , large non-symmetric and non-spherical shells are grown. An example is shown in the inset.

Remarkably, despite the non-equilibrium and stochastic assembly pathways, there were vast regions in the parameter space displaying shells with a high degree of symmetry, see Fig. 4 and Fig. 11. This is due to the interplay between the spontaneous radius of curvature and the response of the elastic triangular network to local stresses. The radius of curvature of a regular icosahedron made up of 20 triangular subunits is  $R_0/b_0 \approx 0.915$  while sheets made of only hexamers are perfectly flat with  $R_0/b_0 = \infty$ . For the range of  $R_0$  studied ( $1.1 < R_0/b_0 < 1.8$ ) in this paper, the introduction of a pentamer creates too much local curvature while the addition of a hexamer will induce too little curvature. Depending which type of capsomers creates more stress we found that the local distortion tended to discourage the formation of similar capsomers in the immediate vicinity of each other. It is this effective repulsion that gives rise to the symmetric structures observed in different systems. Small spontaneous radius of curvature ( $R_0/b_0 < 1.3$ ) promotes formation of pentamers and repulsion between hexamers, leading to the small shells with tetrahedral and dihedral symmetries. Larger  $R_0/b_0$ , on the other hand, favors formation of hexamers and repulsion between pentamers resulting in, for example the  $n_s = 60$  and  $n_s = 80$  subunit shells with icosahedral symmetry.

For large values of spontaneous radius of curvature we were indeed able to obtain similar results to the work of Hicks and Henley(6) and Levandovsky and Zandi(29, 30) both of which used slightly different variants of the model studied in this work. For larger spontaneous radius of curvatures, we obtained mostly irregular capsids with many of the larger capsids displaying defects identical to those observed in Ref. (6). For large shells pertinent to retroviral shells and a fixed FvK number, we found a similar behavior to that seen in Ref. (29), *i.e.*, as spontaneous radius of curvature increased, the type of capsids formed changes from the irregular spheroidal capsids to larger irregular capsids including cone shaped structures to finally tube shaped capsids.

## CONCLUDING REMARKS

In summary we used a minimal non-equilibrium model to study the growth of nano-structures constructed with identical subunits. We found that large spontaneous curvatures between subunits leads to the growth of many small highly symmetric shells, consistent with those observed in nature. The formation of most of the symmetric shells was robust; they were formed over large areas of the parameter space despite the non-reversible and stochastic growth pathways used.

While the mechanical properties of the subunits, described by the single dimensionless FvK number, determined which set of shells was allowed to form as shown in Figs. 5, 6, and 7, the spontaneous radius of curvature determined the size of the shells. For fixed FvK number, the impact of spontaneous curvature on the size and structure of shells was demonstrated in Figs. 8, 9, and 10. These plots clearly indicate that the FvK number  $\bar{\gamma}$  can explain why shells formed from conical particles(11) or clathrin shells(2) display many more magic numbers than the shells formed from viral capsid proteins.

While a large  $\bar{\gamma}$  implies that the subunits are difficult to deform from the preferred shape of an equilateral triangle, small  $\bar{\gamma}$  implies more flexible subunits. The conical particles used in Ref. (11) do not have any explicit triangular symmetry, the underlying hexagonal symmetry only appears due to the close packing of circles in a plane, See Fig. 2. The lack of explicit triangular symmetry leads to a smaller FvK number  $\bar{\gamma}$ , which allows for more diverse shells to be formed. The long legs and



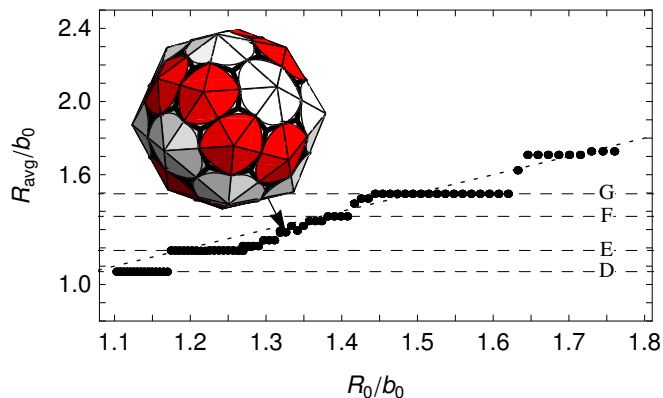


Figure 10: A plot of the average radius  $R_{avg}/b_0$  vs. the spontaneous radius of curvature  $R_0/b_0$ . The FvK number is fixed at a small value of  $\bar{\gamma}=0.25$  corresponding to a flexible subunit. The average radius of the symmetric shells (D), (E) (F) and (G) (see Fig. A.1) are shown with the horizontal dashed lines. The dotted line corresponds to the line where  $R_{avg} = R_0$ . Note that between plateaus corresponding to shell types (E), (F) and (G) there are several non-symmetric shells whose average radius is closer to the spontaneous radius. An example of non-symmetric shell is shown in the inset.

variability of the bonding angle of the triskelion molecules that make up the clathrin results into a more flexible molecule and thus a small FvK number compared to that of viral shells. In contrast to the conical particles employed in simulations and the triskelion molecules in clathrin shells, we expect the viral capsid proteins assume a large FvK number as they only form structures with icosahedral symmetry. It is worth mentioning that while it is widely accepted that the shells with icosahedral symmetry have the lowest free energy structures(7, 11), our work shows that small highly symmetric shells can be reliably formed under non equilibrium conditions and over a wide range of parameter space the *local* minimum free energy path leads to a *global* minimum free energy structure.

A careful analysis of all the structures formed shows that in the range of curvatures studied in this paper, the mismatch between the desired spontaneous radius of curvature and the local radius of curvature induced by a pentamer or hexamer tends to suppress the formation of similar types of capsomers in the vicinity of each other. This suppression tends to lead to the small shells being highly symmetric in nature. This effect seems to be short ranged, which can explain both why larger clathrin vesicles display no symmetry and why larger viruses need scaffolding proteins or other mechanisms to form shells with icosahedral symmetry. While FvK equations can be solved in the absence of spontaneous curvature and give an estimate for the repulsion between pentamers(9), in the presence of spontaneous curvature, the highly non-linear nature of equations makes solving these equations completely non-trivial.

Understanding the mechanisms and assembly pathways of formation of highly symmetric robust shells could have significant impact in the development of anti-viral therapies and in design of novel biomimetic materials.

## APPENDIX A

The symmetric shells assembled through the non-reversible addition of triangular subunits in our work were found to match the symmetric structures in three disparate systems: viral capsids, clathrin coats, and theoretical simulations involving identical cone shaped particles. The shells displayed in Figs. 5, 6, and 7 in the main text are plotted with the relevant subunits to each case in order to best show the match between our work and these systems. However, to provide a consistent comparison between all symmetric shells, we illustrate them all using the same subunit, see Fig. A.1. As clearly revealed in the figure, as the size of shell increases, the strong repulsion between hexamers diminishes and repulsion between pentamers becomes stronger, leading to the shell with different symmetry type. Videos of the step by step growth of each shell is presented in the SI.

## SUPPLEMENTARY MATERIAL

An online supplement to this article can be found by visiting BJ Online at <http://www.biophysj.org>.

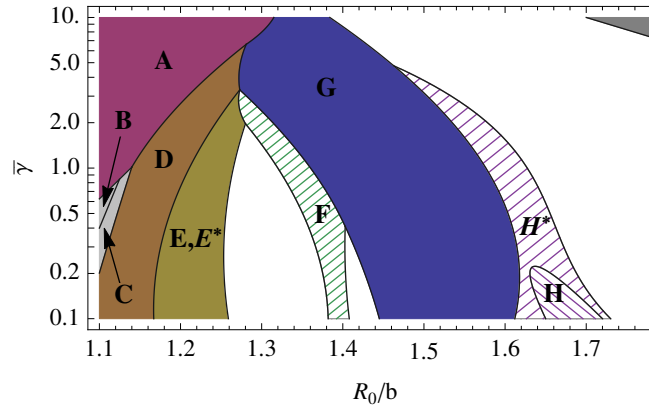


Figure 11: (color online) Phase diagram for the stochastic model with  $\sigma = 20^\circ$  showing the different kind of shells assembled for values of the dimensionless parameters  $\bar{\gamma}$  and  $R_0/b_0$ . In spite of the stochastic growth, only a single shell type is grown in each solid shaded region. However, in the hashed regions several similarly sized non-symmetric shells are formed in addition to the symmetric shell. The white areas correspond to regions where different types of shells without any regular symmetry are assembled. The unlabeled dark shaded area in the upper left corner of the plot with a large FvK number and large spontaneous radius of curvature corresponds to a region in which no pentamers can be formed and the elastic sheet curves around to form a cylinder.

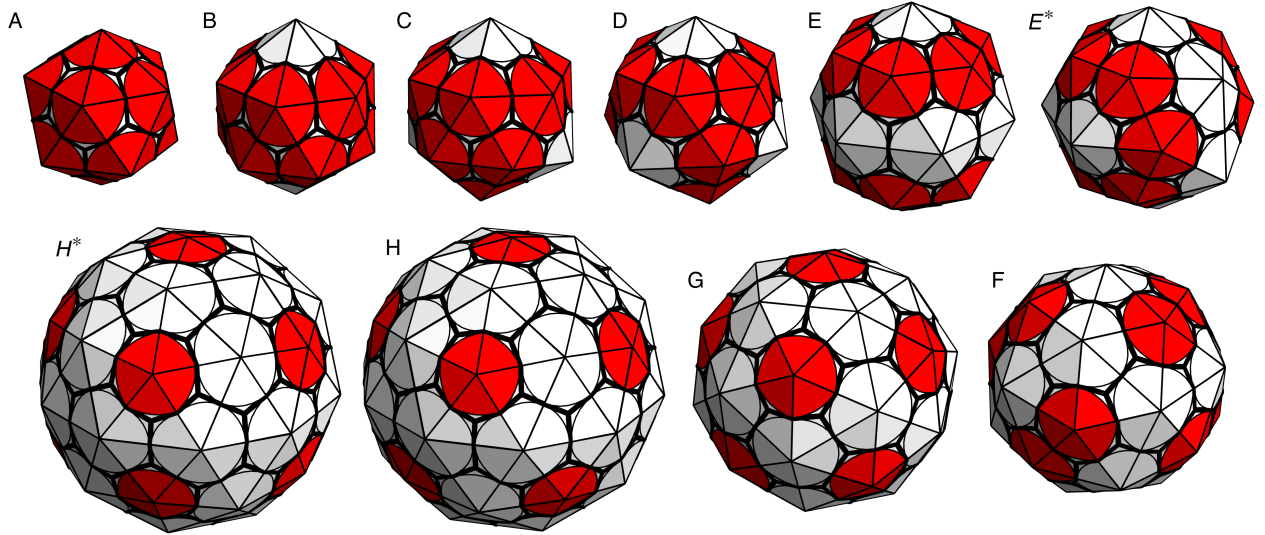


Figure A.1: (color online) The set of small symmetric shells that are formed in the similarly labeled shaded regions in the parameter space plots in Figs. 4 and 11. The subunits are shown as triangles. The pentamers (points with 5 triangles attached) appear darker (red online) in the figure. The shells (A) through (H) have  $n_s = 20, 24, 26, 28, 36, 50, 60$ , and  $80$  subunits or  $N = 12, 14, 15, 16, 20, 37, 32$ , and  $42$  vertices (pentamers and hexamers) respectively. It should be noted that the sets of shells (E) and (E\*), and (H) and (H\*) have the same number of subunits but different symmetries. The symmetries of the shells from left to right and top to bottom are icosahedral,  $D_6$ ,  $D_3$ , tetrahedral,  $D_6$ ,  $D_2$ ,  $D_5$ , icosahedral, icosahedral, and  $S_6$ .

## ACKNOWLEDGMENTS

The authors would like to thank Gonca Erdemci-Tandogan for many helpful discussions. This work was supported by the National Science Foundation through Grant No. DMR-1310687.

## References

1. Crick, F. H. C., and J. D. Watson, 1956. Structure of Small Viruses. *Nature* 177:473.
2. Crowther, R. A., J. T. Pinch, and B. M. F. Pearce, 1976. On the structure of coated vesicles. *J Mol Biol* 103:785.
3. Hogle, J. M., 2012. A 3D framework for understanding enterovirus 71. *Nat Struct Mol Biol* 19:367.
4. Fotin, A., Y. Cheng, P. Sliz, N. Grigorieff, S. C. Harrison, T. Kirchhausen, and T. Walz, 2004. Molecular model for a complete clathrin lattice from electron cryomicroscopy. *Nature* 432:573.
5. Caspar, D. L. D., and A. Klug, 1962. Physical Principles in the Construction of Regular Viruses. *Cold Spring Harbor Symp. Quant. Biol.* 27:1.
6. Hicks, S. D., and C. L. Henley, 2006. Irreversible growth model for virus capsid assembly. *Phys. Rev. E* 74:031912.
7. Zandi, R., D. Reguera, R. F. Bruinsma, W. M. Gelbart, and J. Rudnick, 2004. Origin of icosahedral symmetry in viruses. *PNAS* 101:15556.
8. Bruinsma, R. F., W. M. Gelbart, D. Reguera, J. Rudnick, and R. Zandi, 2003. Viral Self-Assembly as a Thermodynamic Process. *Phys Rev Lett* 90:248101.
9. Lidmar, J., L. Mirny, and D. R. Nelson, 2003. Virus shapes and buckling transitions in spherical shells. *Phys Rev E* 68:051910.
10. Hagen, M. F., and D. Chandler, 2006. Dynamic Pathways for Viral Capsid Assembly. *Biophys J* 91:42.
11. Chen, T., Z. L. Zhang, and S. C. Glotzer, 2007. Simulation studies of the self-assembly of cone shaped particles. *Langmuir* 23:6598.
12. Cadena-Nava, R. D., M. Comas-Garcia, R. F. Garmann, A. L. N. Rao, C. M. Knobler, and W. M. Gelbart, 2012. Self-Assembly of Viral Capsid Protein and RNA Molecules of Different Sizes: Requirement for a Specific High Protein/RNA Mass Ratio. *J Virol* 86:3318.
13. Ni, P., Z. Wang, X. Ma, N. C. Das, P. Sokol, W. Chiu, B. Dragnea, M. Hagan, and C. C. Kao, 2012. An Examination of the Electrostatic Interactions between the N-Terminal Tail of the Brome Mosaic Virus Coat Protein and Encapsidated RNAs. *J. Mol. Biol.* 419:284.
14. Lin, H. K., P. van der Schoot, and R. Zandi, 2012. Impact of Charge Variation on the Encapsulation of Nanoparticles by Virus Coat Proteins. *Phys Biol* 9:066004.
15. Zlotnick, A., 1994. To Build a Virus Capsid: An Equilibrium Model of the Self Assembly of Polyhedral Protein Complexes. *J. Mol. Biol.* 241:59.
16. Siber, A., R. Zandi, and R. Podgornik, 2010. Thermodynamics of nanospheres encapsulated in virus capsids. *Phys Rev E* 81:051919.
17. Manoharan, V. N., M. T. Elsesser, and D. J. Pine, 2003. Dense Packing and Symmetry in Small Clusters of Microspheres. *Science* 301:483–487.
18. Li, C., X. Zhang, and Z. Cao, 2005. Triangular and Fibonacci Number Patterns Driven by Stress on Core/Shell Microstructures. *Science* 309:909–911.
19. Twarock, R., K. ElSawy, A. Taomina, and L. Vaughan, 2008. Dynamical implications of Viral Tiling Theory. *J Theo Biol* 252:357.
20. Lueg, A., D. Reguera, A. Morozov, J. Rudnick, and R. Bruinsma, 2012. Physics of shell assembly: Line tension, hole implosion, and closure catastrophe. *J Chem Phys* 136:184507.
21. Vernizzi, G., and M. Olvera de la Cruz, 2007. Faceting ionic shells into icosahedra via electrostatics. *PNAS* 104:18382–18386.
22. Vernizzi, G., R. Sknepnek, and M. Olvera de la Cruz, 2011. Platonic and Archimedean geometries in multicomponent elastic membranes. *PNAS* 108:4292–4296.
23. Chen, T., Z. Zhang, and S. C. Glotzer, 2007. A precise packing sequence for self-assembled convex structures. *PNAS* 104:717.
24. Schwartz, R., P. W. Shor, P. E. Prevelige, Jr., and B. Berger, 1998. Local Rules Simulation of the Kinetics of Virus Capsid Self-Assembly. *Biophys. J.* 75:2626.
25. Schwartz, R., R. L. Garcea, and B. Berger, 2000. “Local Rules” Theory Applied to Polyomavirus Polymorphic Capsid Assemblies. *Virol.* 268:461.
26. Rapaport, D. C., 2004. Self-assembly of polyhedral shells: A molecular dynamics study. *Phys Rev E* 70:051905.
27. Nguyen, H. D., V. S. Reddy, and C. L. Brooks III, 2007. Deciphering the Kinetic Mechanism of Spontaneous Self-Assembly of Icosahedral Capsids. *Nano Lett* 7:338.
28. Vetterlin, W. T., and B. P. Flannery, 1992. Numerical Recipes in C - The Art of Scientific Computing. Cambridge University Press, 2nd edition. Chapter 10, section 6.
29. Levandovsky, A., and R. Zandi, 2009. Nonequilibrium Assembly, Retroviruses, and Conical Structures. *Phys. Rev. Lett.* 102:198102.
30. Yu, Z., M. J. Dobro, C. L. Woodward, A. Levandovsky, C. M. Danielson, V. Sadrin, J. Shi, C. Aiken, R. Zandi, T. J. Hope, and J. G. J., 2013. Unclosed HIV-1 capsids suggest a curled sheet model of assembly. *J Mol Biol* 425:112–123.